

The Enhanced Photoelectrocatalytic Activity of Ti/Co₃O₄ Nanowires by the Photodeposition of Ag for the Decolorization of Dyeing Wastewater

Yanwei Di^{2,†}, Lu Liu^{3,†}, Xiaoqin Wang², Hongchao Ma^{2,*}, Xuwei Dong^{1,*}, Xinxin Zhang², Yinghuan Fu^{2,*}

¹ School of Environmental and Chemical Engineering, Dalian Jiaotong University, Dalian 116028, China

² School of Light Industry & Chemical Engineering, Dalian Polytechnic University, No.1 Qinggongyuan, Ganjinzi District, Dalian, P.R.China.

³ Dalian University of Technology, No.2 Linggong Road, Ganjingzi District, Dalian City, Liaoning Province, P.R.C., 116024

[†] Authors contributed equally to this work

*E-mail: dxw9872@163.com, fuyinghuan@sina.com

Received: 28 July 2020 / Accepted: 8 October 2020 / Published: 31 October 2020

Co₃O₄ nanowires (NWs) are a promising photoelectrocatalytic (PEC) material; however, they still need to be improved to increase the transport rate and separation efficiency of induced hole/electron pairs, thereby enhancing PEC performance. In this work, we demonstrate that the photodeposition of Ag into Ti/Co₃O₄ NW coatings can promote its PEC ability toward degrading high concentrations of dyeing wastewater. The PEC evaluation shows that the decolorization rate of anthraquinone dye (reactive brilliant blue KN-R) over Ag-modified Ti/Co₃O₄ NWs is 91.7%, which is higher than that of Ti/Co₃O₄ NWs (68.3%). This improvement in PEC activity can be ascribed to Ag-modified Ti/Co₃O₄ NWs having fast carrier transport, a low resistance, a high oxygen evolution overpotential, a large active area and good electron migration efficiency. Moreover, photoelectric synergy can be observed for Ag-modified Ti/Co₃O₄ NWs in the PEC process. The present study provides an effective strategy for the photoelectrochemical treatment of dyeing wastewater by using Ag-modified Ti/Co₃O₄ NWs as an anode.

Keywords: Photoelectrocatalysis, Co₃O₄, dyeing wastewater, Ag modification

1. INTRODUCTION

Wastewater from the textile industry contains a large number of reactive dyes; these dyes have a strong color and high COD levels, making them difficult to degrade and resulting in many environmental problems [1, 2]. For toxic dye wastewater, the main treatment methods are biochemical degradation

[3], ozonation [4], photocatalysis [5-8], adsorption [9] and so on. However, these traditional methods have many disadvantages, such as their poor selectivity, limited degradation capacity, production of secondary pollution, and other issues. Recently, PEC as an efficient method has attracted much attention in the degradation of organic wastewater [10–12]. The PEC process has better separation efficiency of electron/hole pairs by applying an external bias potential to the film electrode, which produces abundant hydroxyl radicals ($\bullet\text{OH}$) [13, 14]. Nevertheless, the photoelectrode material is a key factor for improving the PEC performance, and it is necessary to ensure its sustained high activity and long-term stability. Many materials, such as RuO_2 [15], PbO_2 [16, 17], graphite [18, 19], SnO_2 [20, 21], boron-doped diamond (BDD) [22-24], TiO_2 [25-27], BiVO_4 [28] and Co_3O_4 [29-31], have been used as anodes in PEC systems.

Among numerous materials, Co_3O_4 is a prospective candidate due to its excellent stability, narrow band gap (2.07 eV), high oxygen evolution potential and low cost. Specifically, the one-dimensional Co_3O_4 NWs can maximize the contact area, facilitate electrolyte infiltration and improve the electron transport rate at the electrode/electrolyte interface, which is responsible for improving the PEC activity [32]. However, the degradation efficiency of Co_3O_4 NWs is inhibited by the recombination of induced electron/hole pairs, which has not yet been fully overcome [33]. Previous studies indicated that the surface performance of the catalyst and electron distribution of the system could be changed by the deposition of noble metals, which could provide an effective hybridization effect [34]. Hong et al. prepared Ag-modified Co_3O_4 nanolayers (NLs) by the hydrothermal method, which showed highly efficient PEC activity for water splitting [35]. Zhang et al. prepared Ag/ZnO photocatalysts by photodeposition and found that the photocatalytic activity could be significantly improved [36]. Based on the above references, the PEC performance of a semiconductor can be promoted by modifying with Ag metal because of its superior charge carrier mobility and light absorption performance [37].

In this paper, we combined Ag particles and Co_3O_4 NWs to form a heterostructure and applied it to the degradation of reactive brilliant blue KN-R in a PEC process. The performance of the Ag-modified Ti/ Co_3O_4 NW electrode prepared with different photodeposition times was systematically evaluated in detail. The incorporation of Ag could notably decrease the electronic charge transfer resistance within the electrode and produce a large amount of $\bullet\text{OH}$ on the surface of the photoelectrode, which significantly improved the degradation efficiency of photoelectrocatalysis. In addition, recycling degradation experiments indicated that the fabricated Ag-modified Ti/ Co_3O_4 NW electrode had excellent stability for the decolorization of reactive brilliant blue KN-R.

2. EXPERIMENTAL SECTION

2.1 Reagents

Titanium sheets (99.7% pure) were provided by Yunjiemetal Company (China). $\text{Co}(\text{NO}_3)_2 \cdot 6\text{H}_2\text{O}$, urea, NH_4F , $\text{Ag}(\text{NO}_3)_2$ and reactive brilliant blue KN-R were supplied by Tianjin Chemical Reagents Company. All the required reagents were of analytical grade and could be used

directly without further purification. In this experiment, deionized water was used as a solvent to prepare solutions.

2.2 Electrode preparation

Ti/Co₃O₄ NWs were synthesized by the hydrothermal method, as described in our earlier work[38]. Briefly, the necessary reagents were autoclaved at 120°C for 5 hours and subsequently annealed at 400°C for 2 h (heating rate was 2°C/min), thereby obtaining Ti/Co₃O₄ NWs. AgNO₃ (1 mmol) was dispersed in 190 ml of deionized water. Propyl alcohol (10 ml) was added to the above dispersion under vigorous stirring until the solution was uniform. The Ti/Co₃O₄ NWs were immersed in the AgNO₃ aqueous solution and irradiated with a UV lamp. The distance between the lamp tube and the sample was approximately 2 cm. According to the photodeposition time of Ag on the Ti/Co₃O₄ NW composite, the samples were designated Co, Co-5Ag, Co-10Ag, Co-15Ag, Co-20Ag, Co-25Ag and Co-30Ag. The photodeposition experiments were performed at room temperature.

2.3 PEC experiments

The anthraquinone dye solution (reactive brilliant blue KN-R with a concentration of 0.1 M Na₂SO₄ as a supporting electrolyte) at a concentration of 60 mg L⁻¹ was degraded to appraise the PEC activity of the prepared electrodes. The Ag-modified Ti/Co₃O₄ NW electrode, as the anode, and the titanium sheet, as the cathode, were immersed vertically and parallel in the solution, with a distance of 3 cm between each other. PEC degradation experiments were conducted using a DC current source (current density of 30 mA cm⁻²) and a 15 W UV lamp for photocatalysis. During the experiments, the reaction solution was drawn at certain intervals and analyzed by a UV-visible spectrophotometer (UV-1800PC, MAPADA, China) to measure the degradation rate.

2.4 Characterizations

An X-ray diffraction (XRD) analysis of the electrodes was performed using a SHIMADZU XRD-6100 X-ray diffractometer with a Cu K α radiation source ($\lambda = 0.15406$ nm) and operated at 40 kV and 30 mA. The morphologies of the samples were observed by a scanning electron microscopy (SEM, Hitachi-1510, Hitachi, Japan). In this experiment, we used a CHI660E electrochemical workstation (Chenhua Instruments, Shanghai, China) to carry out electrochemical tests with a standard three-electrode system, in which a platinum plate was used as the counter electrode and a saturated calomel electrode was selected as the reference electrode. In this work, the amount of hydroxyl radicals ($\cdot\text{OH}$) from the PEC decomposition of water was investigated by using fluorescence spectrophotometry (Hitachi F-7000, Japan), the supporting electrolyte was 200 mg L⁻¹ benzoic acid and 0.5 mol L⁻¹ Na₂SO₄ solution.

3. RESULTS AND DISCUSSION

XRD measurements were carried out to identify the crystal structure of the as-prepared samples. In Figure 1, the characteristic diffraction peaks at 2θ values of $38.1^\circ, 44.3^\circ, 64.4^\circ$ and 77.5° correspond to the (111), (200), (220) and (311) crystallographic planes of the Ag phase (JCPDS No:03-0921), respectively, whereas the diffraction peaks at $19.0^\circ, 31.3^\circ, 36.8^\circ, 44.8^\circ, 59.4^\circ$ and 65.2° can be attributed to the (111), (220), (311), (400), (511) and (440) crystal planes of Co_3O_4 (JCPDS No:42-1467), respectively; other diffraction peaks can be indexed to metallic Ti (JCPDS No: 44-1294).

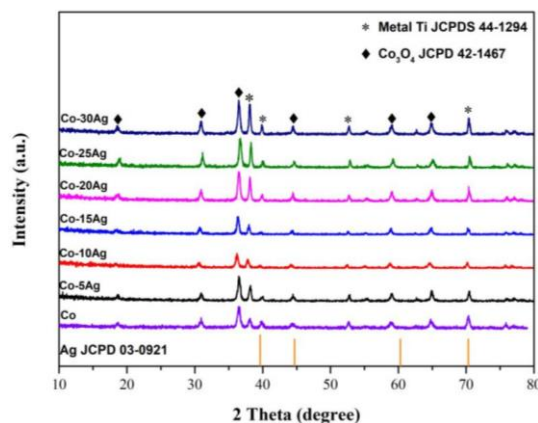


Figure 1. XRD patterns of Ag-modified Ti/ Co_3O_4 NW electrodes with different photodeposition times

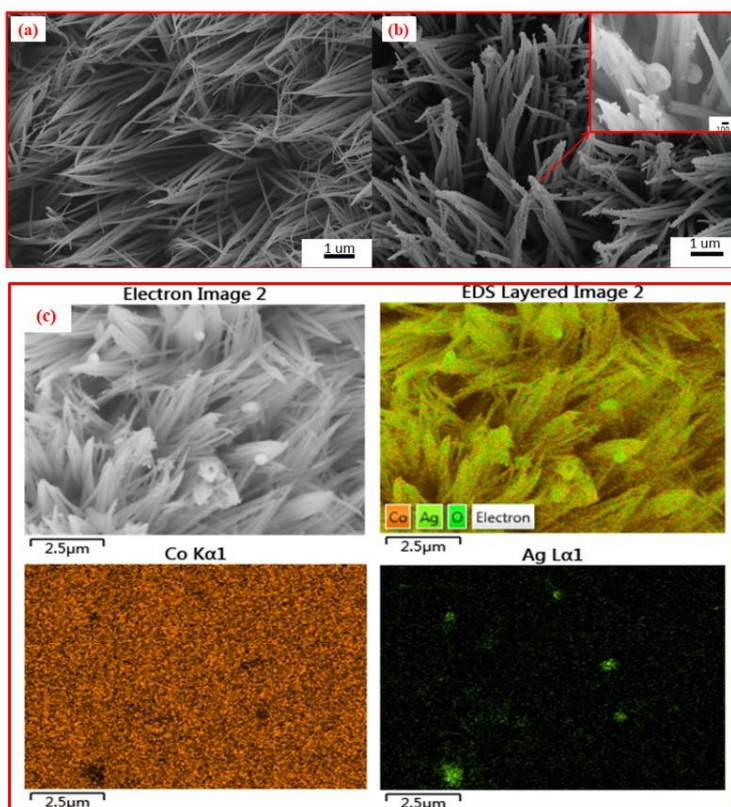


Figure 2. (a-b) SEM images of the bare Ti/ Co_3O_4 NW and Ag-modified Ti/ Co_3O_4 NW electrodes (c) EDS elemental mappings of the Ag-modified Ti/ Co_3O_4 NW electrode.

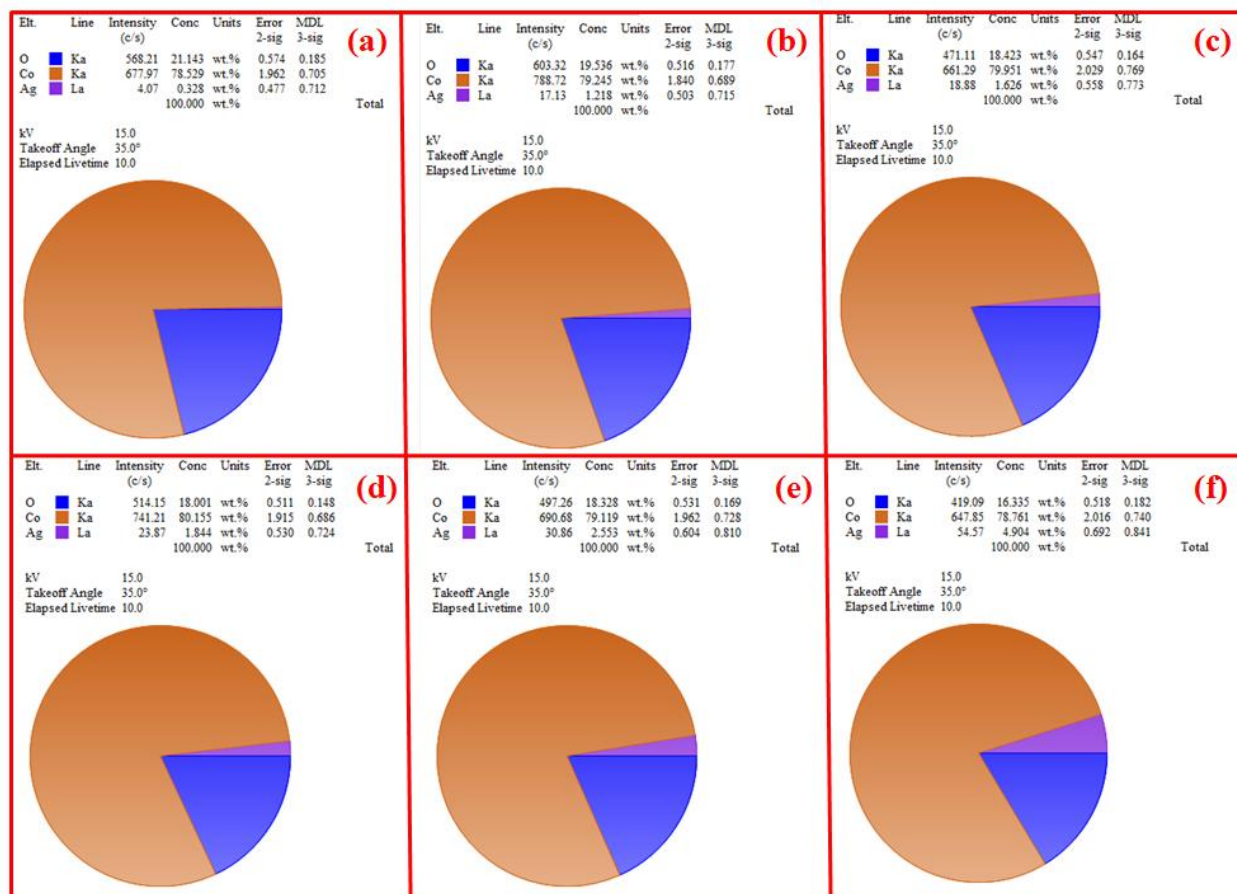


Figure 3. EDX patterns of the Ti/Co₃O₄ NW/Ag electrodes with different photodeposition times: (a) Co-5Ag, (b) Co-10Ag, (c) Co-15Ag, (d) Co-20Ag, (e) Co-25Ag and (f) Co-30Ag.

Moreover, the diffraction peak at 38.2° for Ag is very close to the peaks of the (311) crystal plane of Co₃O₄; thus, the peaks overlap and broaden. Likewise, the diffraction peaks of Ag and Ti overlap at 44.3° and 64.4°, resulting in the intensity of the corresponding peaks for the composite electrode increasing as the Ag content increases.

The SEM images provide direct observations of the surface morphology of the as-prepared electrodes. As shown in Figure 2(a), the bare Ti/Co₃O₄ NWs exhibit a regular needle-like surface with an average diameter of approximately 180 nm and a length of approximately 5.0 μm. In contrast, after the photodeposition of Ag, a mass of Ag particles is observed to adhere on the Ti/Co₃O₄ NW surface (see Figure 2(b)), and the neighboring NWs stick together in clusters, which are prone to providing an abundance of active sites for high reaction activity. The successful heterostructure of Ti/Co₃O₄ NW/Ag was then verified by the high-magnification SEM image (see illustration) in which Ag particles can be observed to tightly combine with Ti/Co₃O₄ NWs. Moreover, the energy-dispersive spectroscopy (EDS) elemental mappings reveal that Ag particles are distributed on the Ti/Co₃O₄ NW surface, as presented in Figure 2(c). The overlapping image of Co, Ag and O provides remarkable evidence of the elemental distribution of Ag on the Ti/Co₃O₄ NW that are on the Ti sheet, which agrees well with the Co and O present in the as-synthesized samples. Thus, the observed Ti/Co₃O₄ NW/Ag heterostructure is beneficial for enhancing electron transport at the electrode, providing an abundance of electrochemically active

sites for improving the PEC activity. With increasing photodeposition time, the content of Ag gradually increases, and the content of Co and O gradually decreases (see Figure 3).

To evaluate the electrochemical properties of the Ti/Co₃O₄ NW/Ag heterostructure electrode, a series of electrochemical measurements were performed by using a three-electrode configuration in a 0.1 M Na₂SO₄ aqueous solution. It is well known that by integrating the area of the cyclic voltammetry (CV) curve (j-E), the number of electroactive sites distributed on the electrode surface can be determined because it is proportional to the determined amount of the voltammetric charge quantity (q*). The CV curves in Figure 4(a) reveal that there is a wide difference between the Ti/Co₃O₄ NWs with and without Ag particles. Note that the closed area of the CV curves for the Co₃O₄ NWs gradually increase with the introduction of Ag. As a result, the q* value of the Ti/Co₃O₄ NW electrodes significantly increases, and a large quantity of electrochemically active sites is introduced to the electrode surface after the Ag deposition. Additionally, the Ag-modified Ti/Co₃O₄ NWs obtained by a 20-min photodeposition show the largest q* value compared with other electrodes. Therefore, the electroactive surface area of the Ti/Co₃O₄ NW electrodes can be enhanced by the introduction of Ag. Subsequently, the Tafel plots of the pure Ti/Co₃O₄ NWs and Ag-modified Ti/Co₃O₄ NWs are shown in Figure 4(b). The Tafel slope is a crucial metric regarded as an inherent property of electrocatalysts. A small Tafel slope represents a fast electron transfer rate with increasing potential[39]. As expected, the introduction of Ag on the Ti/Co₃O₄ NWs show a smaller Tafel slope than pure Co₃O₄ NWs. The Tafel slope of the catalyst is as low as 269 mV/decade, which is much smaller than that of other catalysts. Therefore, the Co-20Ag electrode exhibits good PEC activity.

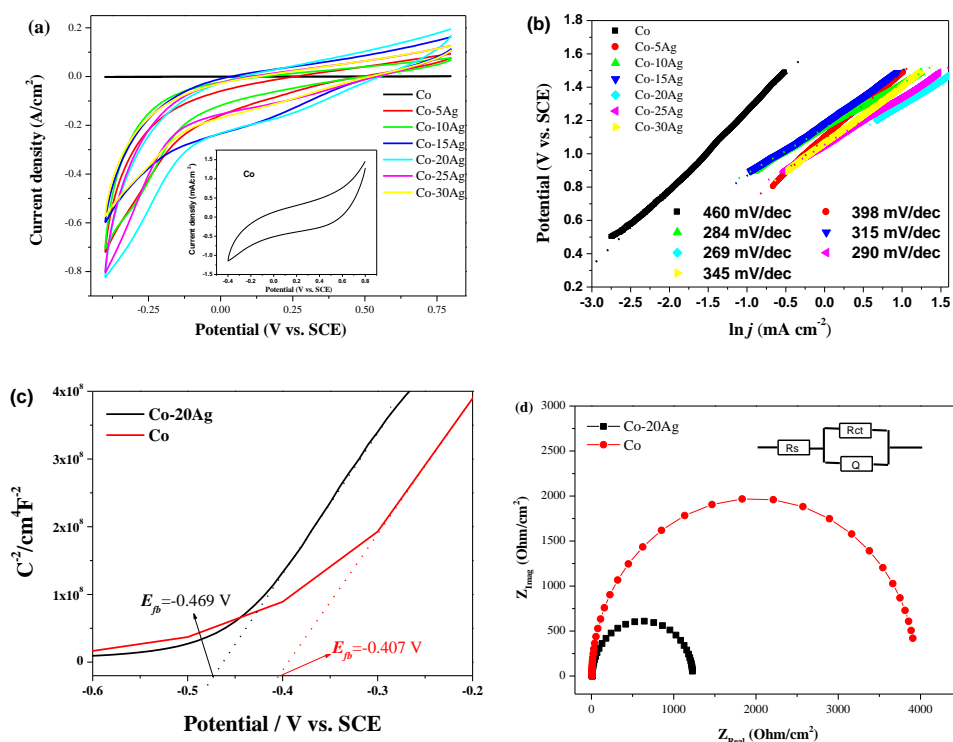


Figure 4. (a) Cyclic voltammograms, (b) linear sweep voltammetry curves, (c) Mott-Schottky plots and (d) Nyquist plots of the Ti/Co₃O₄ NW and Ag-modified Ti/Co₃O₄ NW electrodes in a 0.1 M Na₂SO₄ solution without light.

To determine the type of semiconductor and calculate the carrier concentration (N_D values) of the as-prepared samples, Mott-Schottky plots of the Ti/Co₃O₄ NW and Ti/Co₃O₄ NW/Ag heterostructures are shown in Figure 4(c). In the Mott-Schottky diagram, the positive slope of the linear portion of the curve indicates that the two materials are n-type semiconductors. Some researchers have suggested that an n-type semiconductor with a more negative flat band potential (E_{fb}) possesses better electrocatalytic activity. The E_{fb} of the Ti/Co₃O₄ NW and Ti/Co₃O₄ NW/Ag electrodes are found to be -0.407 V and -0.469 V, respectively. Evidently, the large negative shift of E_{fb} for Ti/Co₃O₄ NW/Ag can be attributed to electronic storage at the heterostructure interface. Thus, the existence of Ag may be beneficial for promoting efficient electrocatalytic activity. In addition, N_D values can be calculated using the following equation:

$$\frac{1}{c^2} = \frac{2}{N_D e \epsilon_0 \epsilon} \left(E - E_{fb} - \frac{kT}{e} \right)$$

where c is the capacitance of the space charge layer for the semiconductor, N_D is the carrier density of the electrons, e (1.6×10^{-19} C) is the value of the elementary charge, ϵ_0 (8.86×10^{-12} F/m) is the permittivity of the vacuum, ϵ is the relative permittivity of the semiconductor, E is the applied bias, E_{fb} is the band potential, k is the Boltzmann constant, and T is the temperature.

Nyquist plots from electrochemical impedance spectroscopy (EIS) data is a vital tool used to research the interfacial properties between the electrode and the solution. Figure 4(d) displays the EIS results of these two samples. The illustration shows the equivalent circuit of the electrochemical devices, which can analyze the reaction mechanisms involved in the electrode process, where R_s , R_{ct} and Q are the series resistance, charge transfer resistance and constant phase element, respectively. It is reported that on the EIS Nyquist curve, the size of the semicircle diameter reflects the reaction rate taking place on the surface. That is, a small arc radius represents a fast redox reaction proceeding on the electrode surface. It is thus apparent that the photodeposition of Ag on the Ti/Co₃O₄ NW surface is more favorable for quick charge transfers as well as fast ion exchanges between the electrode/electrolyte interface, consistent with the above electrochemical results.

The effect of the Ag content on the photoelectrocatalytic performance of the prepared Ti/Co₃O₄ NW samples was examined. In this work, the quantity of hydroxyl radicals (\bullet OH) during electrolysis was explored by obtaining photoluminescence (PL) spectra. Figure 5(a) shows the PL spectra of a benzoic acid solution over each electrode at different electrolysis times (0-120 min). The Ag-modified Ti/Co₃O₄ NW electrodes exhibit strong fluorescence intensity at all times, which indicates that the as-prepared electrodes can generate more \bullet OH. In particular, the Ti/Co-20Ag electrode exhibits the highest fluorescence intensity during the whole period. However, the further addition of Ag content (Ti/Co-25Ag and Ti/Co-30Ag) results in a lower PL intensity compared with that of the Ti/Co-20Ag electrode, which may possibly be due to having too many Ag particles covering the active sites. This result further proved that the existence of Ag on the electrode may be beneficial for promoting PEC activity to indirectly degrade organic pollutants. It is clear from Figure 5(b) that the KN-R degradation in simulated dye wastewater is proportional to the reaction time and that the introduction of Ag shows a remarkable effect on the PEC performance. During the experiment, the effective area of the electrode is 4 cm², and the current density is 30 mA/cm². Typically, the efficiency of PEC on KN-R degradation is promoted by the addition of a small amount of Ag (5 min-20 min), and the Co-20Ag composite shows the highest

PEC activity, up to 91.7%. However, when the Ag content on the Ti/Co₃O₄ NW electrode is further increased, the degradation efficiency exhibits a decreasing trend. Based on previous reports, this phenomenon may be due to the excessive decoration of Ag destroying the Ti/Co₃O₄ NW active sites, thus reducing the PEC performance of the Ti/Co₃O₄ NW/Ag electrodes. The KN-R removal with various degradation processes, including electrocatalytic (EC), photocatalytic (PC) and PEC processes, are summarized in Figure 5(c). The photoanode does not show obvious EC activity when the electrolysis potential range is 1.5–3.0 V, and the PEC process is almost equal to the sum of both EC and PC. Notably, the PEC process exhibits the highest degradation efficiency when the current density is 30 mA/cm² and the electrolysis voltage reaches 11.4 V. Remarkably, the degradation efficiency of the PEC process is higher than the summation of the individual PC and EC processes. As a result, there is a synergistic effect in the PEC process. The energy consumption (kWh kg⁻¹) of KN-R degradation is used to appraise the optimal conditions of degradation. The energy consumption of KN-R degradation can be defined as:

$$EC = \frac{1000Ut}{(C_0 - C_t)V_s}$$

where U is the applied voltage (Volt), I is the applied current (Ampere), t is the degradation time (hour), $(C_0 - C_t)$ is the concentration of removed KN-R (mg/L) and V_s is the volume of the solution (Liter). The removal rates and energy consumption values of degrading KN-R over the Co-20Ag sample under different degradation conditions are shown in Figure 5(d).

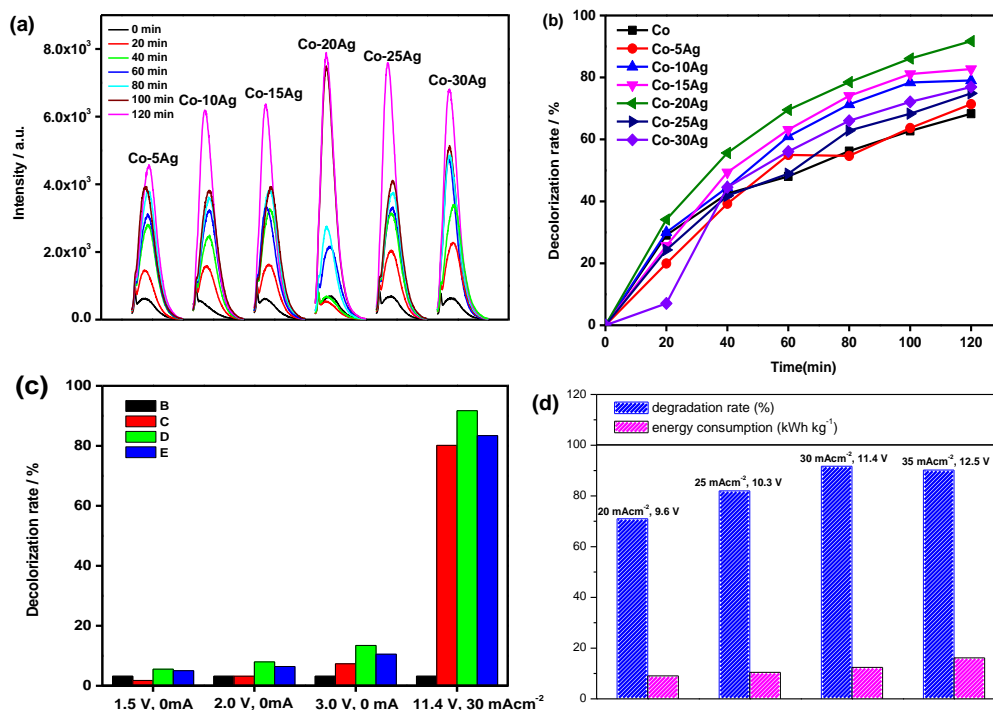


Figure 5. (a) Fluorescence spectra of benzoic acid (200 mg L⁻¹ benzoic acid and 0.5 mol L⁻¹ Na₂SO₄ as the supporting electrolyte). (b) Degradation rate of the bare Ti/Co₃O₄ NW and Ti/Co₃O₄ NWs/Ag electrodes for reactive brilliant blue KN-R during the PEC process. (c) Photoelectric synergy of the Ti/Co-20Ag electrode (the comparison of EC, PC and PEC), (d) Energy consumption of the Ti/Co-20Ag electrode sample for the degradation of reactive brilliant blue KN-R under different degradation conditions.

In the above discussion, the PEC activity of the prepared electrode was evaluated by the degradation of reactive brilliant blue KN-R under simulated sunlight irradiation. Thus, to further understand the excellent electrocatalytic activity of the prepared electrode, the PEC activity of the prepared electrode in this text was compared with those previously reported literature. Ma et al. fabricated F-doped Ti/Co₃O₄ electrodes by a typical hydrothermal process and showed a degradation rate of 84% for active brilliant blue after 2 hours [38]. Wang et al. constructed PbO₂/Co₃O₄ composite electrodes by the combination of a hydrothermal synthesis and an electrochemical deposition. This kind of electrode exhibited a degradation rate of 82.7% for active brilliant blue after 2 hours [33]. Among the reported modification methods of Co₃O₄ in the above literature, its PEC activity was not as high as that of the Ag deposition methods (degradation rate of 91.7% for active brilliant blue). In addition, Zhang et al. reported that the Co₃O₄/Ag/TiO₂ composite nanotube electrode prepared by the photoreduction of Ag and the thermal decomposition of Co₃O₄ nanoparticles also showed excellent catalytic activity for the removal of NB and Cr(VI), which further proved that the deposition of Ag could significantly improve the PEC performance of Co₃O₄ [40].

Based on previous theoretical studies [41-43], a possible mechanism for the PEC degradation of the Ti/Co₃O₄NW/Ag heterostructure is proposed. From the image shown in Figure 6, the photoinduced electrons are excited to the conduction band (CB) of the Ti/Co₃O₄NW/Ag nanocomposites (NPs) under UV-light irradiation and then accumulate on the Ag particle surface due to the surface plasmon resonance (SPR) effect. In detail, the Fermi level [34] of Ag NPs is lower than the CB of the samples, and the loaded Ag NPs act as electron traps that accumulate electrons to form a high Schottky barrier that exists at the sample interface. Additionally, the photoexcited electrons have good fluidity and are transferred to the cathode by an external bias potential (the applied potential is greater than the flat-band potential) in the PEC cell device or can easily transfer to the absorbed O₂ on the Ag surface, forming O₂⁻ active groups, which significantly inhibit the recombination of electron holes. Moreover, excited holes can easily be transferred into the surface from the valence band (VB) and subsequently react with adsorbed water to form ·OH. Additionally, low-dimensional nanostructures, the needle-like NWs of Co₃O₄ NWs can also provide direct pathways for the migration of photogenerated electrons, thus facilitating charge-carrier separation that can significantly enhance the PEC activity of the photoanode to degrade organic pollutants in wastewater.

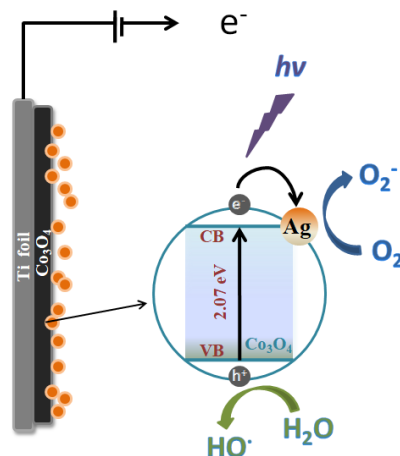


Figure 6. Diagram of the energy band and charge transfer mechanism of the Ag-modified Ti/Co₃O₄ NW heterostructure.

4. CONCLUSIONS

In summary, a Ti/Co₃O₄ NW/Ag electrode with outstanding PEC performance is demonstrated by degrading dyeing wastewater (reactive brilliant blue KN-R) when used as the anode. The advanced heterostructure favors fast ion/electron transport and ensures a sufficient active area because it integrates advantageous properties, including a large specific surface area, high oxygen evolution potential and low resistance. Moreover, the construction of the as-prepared heterostructure can facilitate an improved electron (e⁻)/hole (h⁺) pair separation rate and reduce recombination during the PEC process. As a consequence, the photoanode displays an extremely high decolorization of dyeing wastewater (the decolorization rate of KN-R reaches 91.7% after 120 min), compared with that of bare Ti/Co₃O₄ NWs (the decolorization rate of KN-R is only 71.1% after 120 min), and long-term cycling durability. More importantly, forming an effective hybrid structure improves the PEC synergistic effect. This work provides enlightening insights for modification of electrode surface and rapid separation of photogenerated carriers.

ACKNOWLEDGMENTS

This work was supported by the National Natural Science Foundation of China (21875026, 21878031), the Program for Liaoning Excellent Talents in University (LR2014013), the Natural Science Foundation of Liaoning Province (NO.20170520427), the Science and Technology Foundation of Liaoning Province (NO.201602052), and supported by Liaoning Revitalization Talents Program (XLYC1802124). The Project was sponsored by the scientific research fund of the educational department of Liaoning province (J2019013) and Liaoning BaiQianWan Talents Program. This work was also supported by Joint Research Fund Liaoning-Shenyang National Laboratory for Materials Science (Project Number: 2019JH3/30100034; Contract Number: 2019010278-JH3/301).

References

1. B. K. Korbahti, A. Tanyolac, *J. Hazard. Mater.*, 151 (2008) 422.
2. V. M. Correia, T. Stephenson, S. J. Judd, *Environ. Technol.*, 15 (1994) 917.
3. S. Pramanik, S. Chaudhuri, *Mycobiology*, 46 (2018) 79.
4. S. Barredo-Damas, M. I. Iborra-Clar, A. Bes-Pia, M. I. Alcaina-Miranda, J. A. Mendoza-Roca, A. Iborra-Clar, *Desalination*, 182 (2005) 267.
5. S. H. S. Chan, T. Yeong Wu, J. C. Juan, C. Y. Teh, *J. Chem. Technol. Biotechnol.*, 86 (2011) 1130.
6. H. Wang, L. Xiao, C. Wang, B. Lin, S. Lyu, X. Chu, Y. Chi, X. Yang, X. Wang, *Chem Res Chinese U.*, 35 (2019) 667.
7. J. Wang, Y. Yi, M. Li, Y. Chang, F. Zha, *Chem Res Chinese U.*, 35 (2019) 319.
8. Y. Liu, Y. Chu, Z. Du, Y. Sun, F. Cao, *Chem Res Chinese U.*, 35 (2019) 662.
9. J. Paprowicz, S. Słodczyk, *Environ. Technol. Lett.*, 9 (1988) 271.
10. Y. Han, X. Ruan, J. Chen, H. Zhang, H. Zhao, S. Zhang, *Asian J. Chem.*, 25 (2013) 6167.
11. G. Chen, *Sep. Purif. Technol.*, 38 (2004) 11.
12. E. O. Scott-Emuakpor, A. Kruth, M. J. Todd, A. Raab, G. I. Paton, D. E. Macphee, *Appl. Catal.*, B, 123-124 (2012) 433.
13. Y. Ghayeb, M. M. Momeni, E. Ghonjalipoor, *Appl. Phys.*, A, 125 (2019).
14. M. G. Peleyeju, O. A. Arotiba, *Environ Sci-Wat Res*, 4 (2018) 1389.
15. D. Gong, J. Zhu, B. Lu, *RSC Adv.* 6 (2016) 49173.
16. R. Amadelli, L. Samiolo, A. D. Battisti, A. B. Velichenko, *J. Electrochem. Soc.*, 158 (2011) P87.
17. D. V. Girenko, A. B. Velichenko, E. Mahé, D. Devilliers, *J. Electroanal. Chem.*, 712 (2014) 194.
18. Y. Kong, Z.-l. Wang, Y. Wang, J. Yuan, Z.-d. Chen, *Carbon*, 50 (2012) 2063.
19. J. M. Skowronski, P. Krawczyk, *J. Solid State Electrochem.*, 8 (2004) 442.
20. Y. Wang, Y. Chen, H. Zhu, X. Zhang, *Trans. Tianjin Univ.*, 22 (2016) 247.
21. H. An, H. Cui, W. Zhang, J. Zhai, Y. Qian, X. Xie, Q. Li, *Chem Eng J*, 209 (2012) 86.
22. A. Dirany, I. Sires, N. Oturan, A. Ozcan, M.A. Oturan, *Environ. Sci. Technol.*, 46 (2012) 4074.
23. A. Thiam, I. Sirés, J. A. Garrido, R. M. Rodríguez, E. Brillas, *Sep. Purif. Technol.*, 140 (2015) 43.
24. A. Fabianska, A. Bialk-Bielinska, P. Stepnowski, S. Stolte, E. M. Siedlecka, *J. Hazard. Mater.*, 280 (2014) 579.
25. L. Zhu, H. Ma, H. Han, Y. Fu, C. Ma, Z. Yu, X. Dong, *RSC Adv.*, 8 (2018) 18992.
26. S. Kuang, L. Yang, S. Luo, Q. Cai, *Appl. Surf. Sci.*, 255 (2009) 7385.
27. Y. Hou, X. Y. Li, Q. D. Zhao, X. Quan, G. H. Chen, *Appl. Phys. Lett.*, 95 (2009) 093108.
28. R. Abe, *J. Photochem. Photobiol.*, C, 11 (2010) 179.
29. X. Huang, T. Cao, M. Liu, G. Zhao, *J. Phys. Chem. C*, 117 (2013) 26432.
30. Y. Mao, W. Li, P. Liu, J. Chen, E. Liang, *Mater. Lett.*, 134 (2014) 276.
31. J. Mei, T. Liao, G.A. Ayoko, J. Bell, Z. Sun, *Prog. Mater. Sci.*, 103 (2019) 596.
32. J. Liu, J. Jiang, C. Cheng, H. Li, J. Zhang, H. Gong, H. J. Fan, *Adv. Mater.*, 23 (2011) 2076.
33. X. Wang, Q. Wu, H. Ma, C. Ma, Z. Yu, Y. Fu, X. Dong, *Sol. Energy Mater. Sol. C*, 191 (2019) 381.
34. S. Linic, P. Christopher, D. B. Ingram, *Nat Mater*, 10 (2011) 911.
35. T. Hong, Z. Liu, X. Zheng, J. Zhang, L. Yan, *Appl. Catal.*, B, 202 (2017) 454.
36. Z. Zhang, H. Liu, H. Zhang, H. Dong, X. Liu, H. Jia, B. Xu, *Superlattices Microstruct.*, 65 (2014) 134.
37. X. Zhang, B. Lu, R. Li, X. Li, X. Gao, C. Fan, *Sep. Purif. Technol.*, 154 (2015) 68.
38. H. Ma, X. Wang, Y. Fu, Y. Zhang, C. Ma, X. Dong, Z. Yu, *J. Solid State Electrochem.*, 23 (2019) 1767.
39. S. P. Lim, A. Pandikumar, N. M. Huang, H. N. Lim, *Int. J. Hydrogen Energy*, 39 (2014) 14720.
40. Y. Zhang, J. Nie, Q. Wang, X. Zhang, Q. Wang, Y. Cong, *Appl. Surf. Sci.*, 427 (2017) 1009.
41. N. Hu, W. H. Gong, L. Huang, P. K. Shen, *J. Mater. Chem. A*, 7 (2019) 1273.
42. G. Luo, X. Jiang, M. Li, Q. Shen, L. Zhang, H. Yu, *ACS Appl. Mater. Interfaces*, 5 (2013) 2161.

43. X. Li, S. Fang, L. Ge, C. Han, P. Qiu, W. Liu, *Appl Cataly-B Environ*, 176-177 (2015) 62.

© 2020 The Authors. Published by ESG (www.electrochemsci.org). This article is an open access article distributed under the terms and conditions of the Creative Commons Attribution license (<http://creativecommons.org/licenses/by/4.0/>).